National Ilan University
國立宜蘭大學工程學刊第8期，78-89頁，2012年12月
Bulletin of College of Engineering National Ilan University No. 8, P. 78-89, December 2012
Bulletin of College of Engineering
http://engineering.niu.edu.tw/main.php

# 磨耗尖鼻負稜碳化鎢車刀切削碳纖複合材料(CFRP)之溫度預測研究

張充鑫[1] 陳正虎[2]

1.國立宜蘭大學機械工程學系與機電工程學系（所）教授
2.國立宜蘭大學機械工程學系與機電工程學系（所）副教授

## 摘要

本研究是一種選用 K 型材質的尖鼻負稜主刃碳化鎢車刀片，當刀尖在工具磨床上預先磨有一磨耗量後，針對碳纖維複合材料(CFRP)做車削研究。研究當中除了量測三軸切削力外，並利用切削過程中，刀面與工件之摩擦面積，以計算出摩擦力。其次配合有限元素分析技術(FEA)，利用 Abqus™ 軟體及逆向分析法 (Inverse method)，以預測磨耗尖鼻負稜碳化鎢車刀切削碳纖複材時其刀尖之表面溫度。最後與紅外線儀器所量測的結果作比較，結果顯示量測值與預測值很接近。

**關鍵詞**：車削、切削溫度、碳纖複材、有限元素分析(FEA)

***通訊作者E-mail：cschang@niu.edu.tw**

National Ilan University

國立宜蘭大學工程學刊第8期，78-89頁，2012年12月
Bulletin of College of Engineering National Ilan University No. 8, P. 78-89, December 2012

Bulletin of College
of Engineering
http://engineering.niu.edu.tw/main.php

# Prediction of Cutting Temperatures in Turning Carbon-Fiber-Reinforce-Plastics Materials Using Chamfered Main Cutting Edge Sharp Tools Considering Wear

**Chung-Shin Chang[1], Cheng-Hu Chen[2]**

1. Professor, Department of Mechanical and Electro-Mechanical Engineering, National Ilan University
2. Associate Professor, Department of Mechanical and Electro-Mechanical Engineering, National Ilan University

## ABSTRACT

Temperatures of the carbide tip's surface when turning Carbon-Fiber-Reinforced-Plastics (CFRP) materials with a K type sharp main cutting edge tool considered wear is investigated. The frictional forces and heat generated in the basic cutting tools are calculated by using the measured cutting forces and the theoretical cutting analysis. The heat partition factor between the tip and chip is solved by using the inverse heat transfer analysis, which utilizes temperature on the carbide tip's surface measured by infrared as the input. The carbide tip's surface temperature is determined by finite element analysis (FEA, Abaqus™ software) and compared with temperatures obtained from experimental measurements by infrared . Good agreement demonstrates the proposed model.

**Keywords:** Turning, cutting temperatures, CFRP, FEA.

***Corresponding author E-mail: cschang@niu.edu.tw**

## 1. INTRODUCTION

Singamneni (2005) demonstrated the mixed finite and boundary element method (FEM) finally enables the estimation of the cutting temperatures which is a simple, efficient method, and at the same time it is quite easy to be implemented. The objective of this paper is to set up an oblique cutting CFRP model to study three-dimensional cutting temperature for a sharp worn tool with a chamfered main cutting edge.

## 2. THEORETICAL ANALYSIS

Bhatnagar et al. (1995) showed that in machining of fiber reinforced plastic (FRP) composite laminates; it can be assumed that the shear plane in the matrix depends only on the fiber orientation and not on the tool geometry. Chang (2008) presented a model to predict the cutting temperatures in turning of glass-fiber-reinforced plastics with chamfered main cutting edge sharp worn tools that can accurately predict the cutting temperatures and the cutting forces. For the case of chamfered main cutting edge, temperatures and forces depend on nose radius *R*, first side rake angle $\alpha_{S1}$, second side rake angle $\alpha_{S2}$, as shown in Fig.1 and Table 1.

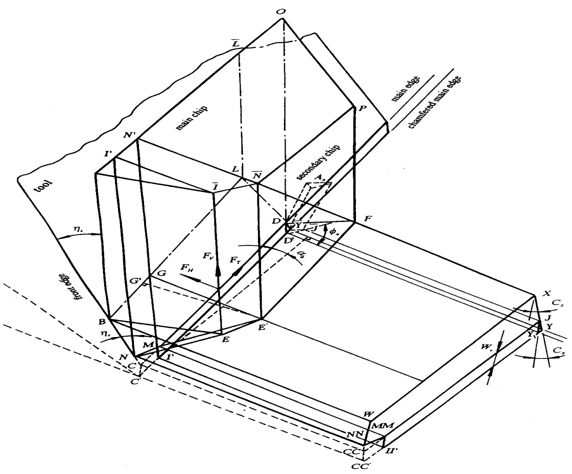


Figure 1. Basic model of the chamfered main edge.

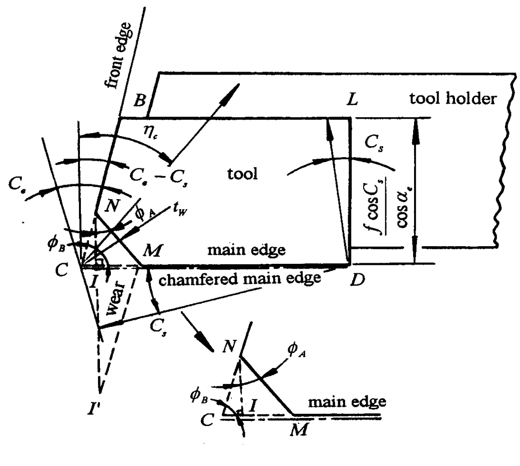


Figure 2. Specifications of tool face with wear tool when wear (f > R, R≠0).

## 2.1 Shear Area in the Cutting Process with Chamfered Cutting Edge Sharp Tools Considering Wear

Fig. 2 reveal that the geometrical specification of tool wear on the tool face (triangle $CN$M) can be derived from the values of $t_W$ and $\varphi_A$ when already measured.

$$A = A_1 + A_2 + A_3 + A_S \text{ (as shown in Fig.1)} \tag{1}$$

$$A_1 = 0.5a_3b_3 \sin\theta_3 = 0.5a_3b_3 \quad [1-(a_3{}^2+b_3{}^2-c_3{}^2)/2a_3b_3]^{1/2}\}\,(A_1 = \Delta NBE) \tag{2}$$

$$A_2 = \frac{1}{2}(a_4+b_4)\cdot h_4\,(A_2 = \text{rectangle}\,MDFE') \quad (3), \quad A_3 = A_{31}+A_{32} \quad (A_3 = \Delta ME'E + \Delta MNE) \quad (4)$$

$$A_{31} = \frac{a_5b_5}{2\cos\phi_e}\sin\left(\frac{0.5\pi+\alpha_b-\angle A31}{2}\right) \quad (5), \quad \angle A31 = \cos^{-1}\left[\frac{c_5{}^2+d_5{}^2-e_5{}^2}{2c_5d_5}\right] \quad (6)$$

$$A_{32} = g_5h_5\,\frac{\sin(\angle A32)}{2\cos\phi_e} \quad (7) \quad \angle A32 = \cos^{-1}\left[\frac{h_5{}^2+n_5{}^2-m_5{}^2}{2h_5n_5}\right] - \sin^{-1}\left[\frac{l_5}{s_5}\sin\left(\frac{\pi}{2}-\alpha_b\right)\right] \quad (8)$$

$$A_s = (0.5W_e{}^2\cos^2\alpha_{s1}\tan C_s)/(\cos\alpha_b\sin\phi_e)\,(A_S \text{ is the area of secondary chip:} \Delta D'\overline{YJ}\,) \tag{9}$$

$$Q = Q_1 + Q_2 + Q_3 \tag{10}$$

$$Q_1 = \frac{0.5(d/\cos C_s - W_e\cos^2\alpha_{s1}\tan C_s)}{\cos\alpha_b}\cdot\frac{f\cos C_s - W_e\cos\alpha_{s1}}{\cos\alpha_{s2}} - (\overline{CN}\cdot\overline{NM}\sin\phi_B)/0.5 \tag{11}$$

$$Q_2 = \frac{W_e\cos\alpha_{s1}(d/\cos C_{s1}\tan C_s)}{\cos\alpha_b} - \overline{CN}\cdot W_e\cos\alpha_{s1} \quad (12), \quad Q_3 = (0.5W_e{}^2\cos\alpha_{s1}\tan C_s)/\cos\alpha_b \quad (13)$$

$$\overline{CM} = t_W(\cos C_S + \sin C_S\tan\phi_A) \quad (14), \quad \overline{CN} = \frac{t_W(\cos C_S + \sin C_S\cdot\tan\phi_A)}{(\sin\phi_A\tan\phi_A + \cos\phi_B)} \quad (15)$$

$$\overline{NM} = (\overline{CM}^2 + \overline{CN}^2 - 2\overline{CM}\cdot\overline{NM}\cos\phi_B)^{1/2} \tag{16}$$

$$\angle CMN = \cos^{-1}\left[\frac{(\overline{CM}^2+\overline{CN}^2-\overline{NM}^2)}{2\overline{CM}\cdot\overline{CN}}\right] \quad (17), \quad \angle CNM = \cos^{-1}\left[\frac{(\overline{CN}^2+\overline{NM}^2-\overline{CM}^2)}{2\overline{CN}\cdot\overline{NM}}\right] \quad (18)$$

The contact length of the tool edge can be considered as in Fig. 2.

$$\overline{NM}\cos\left(\frac{\pi}{2}-\angle CMN\right) < \left(\frac{f\cos C_s}{\cos\alpha_e} - W_e\cos\alpha_{S1}\right)$$

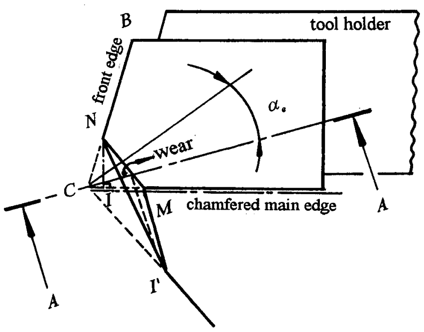


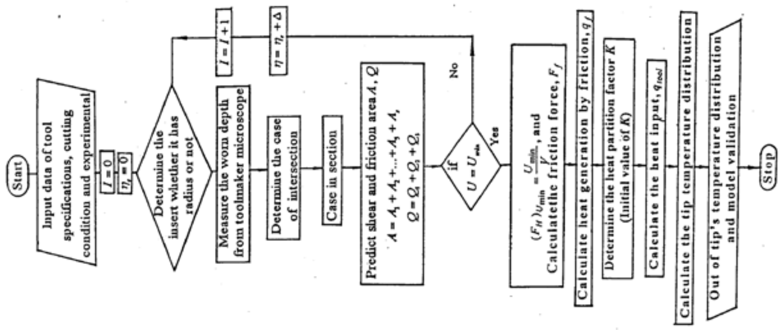

Figure 3. Tool tip wears with chamfered main cutting edge tool.

Figure 4. Flow chart of the inverse heat transfer

From the above diagram, the contact length is $l_f = \overline{HN} + \overline{NM} + \overline{MD} = \bar{i} \cdot \overline{ii} + \overline{ii} \cdot \overline{iii} + \overline{iii} \cdot \overline{iv} =$

$$[\frac{f\cos C_s / \cos\alpha_e) - W_e \cos\alpha_{s1})}{\cos(C_e - C_s)} + \overline{NM} + \frac{d}{\cos C_s \cos\alpha_b} - \overline{CM} \tag{19}$$

$$l_p = \overline{HN}\cos C_e + \overline{NM}\cos(\angle CNM - C_e) + \overline{MD}\sin C_s\,[\frac{f\cos C_s - W_e\cos\alpha_{s1})}{\cos\alpha_e\cos(C_e - C_s)} + \overline{NM}\cos(\angle CNM - C_e) +$$

$$(d/\cos C_s - \overline{CM})\sin C_s \tag{20}$$

**2.2. Energy Method to Predict Cutting Force**

Transformation equations used to obtain the normal ($N_s$) and shear forces ($F_s$) along the fiber direction in terms of the principal ($F_c$) and thrust components ($F_t$) are shown in Eqs. (21) and (22).

$N_S = F_c \sin\theta + F_t \cos\theta$ (21), $F_S = F_c \cos\theta + F_t \sin\theta$, Liu (2002) (22)

$\tau_S = \tau_{compsite} = \tau_{fiber} V_f$ by Rosen and Dow(1987) ($V_f$ is fiber contains)

$V_S = V\cos\alpha_e / \cos(\varphi_e - \alpha_e)$, (23), $f_t = \tau_S t_1 \sin\beta / \cos(\varphi + \beta - \alpha)\sin\varphi$ (24)

$V_C = V\sin\varphi_e / \cos(\varphi_e - \alpha_e)$ (25) $\alpha_e = \sin^{-1}(\sin\alpha_{S2}\cos\alpha_b\cos\eta_C + \sin\eta_C\sin\alpha_b)$ (26)

Therefore, $(F_H)_{Umin}$ was determined by solving Equ. (28) in conjunction with the energy method by Reklaitis etc.(1984). (27)

$$F_{H}=\frac{U_{\min}}{V}=\{\frac{\tau_S\cos\alpha_e A}{\cos(\varphi_e-\alpha_e)}+\frac{\tau_S\sin\beta\cos\alpha_e Q}{\cos(\varphi_e+\beta-\alpha_e)\cos(\varphi_e-\alpha_e)}$$ (28), where the frictional force is

determined by $F_t=\frac{\tau_s \sin\beta\cos\alpha_e Q}{[\cos(\phi_e+\beta-\alpha_e)\sin\phi_e]}$ (29)

$$N_t=\frac{[(F_H)-(F_t)_{U_{\min}}\sin\alpha_e]}{\cos\alpha_{S2}\cos\alpha_b} \quad (30)$$

### 2.3. Calculation of Flank Wear

Thus, the flank wear $V_B$ is a function of $t_W$, $\theta_e$ and $\alpha_e$. $V_B=t_W\cos\alpha_e(\cot\theta_e-\tan\alpha_e)$ (31)

### 2.4. Finite Element Model

The finite element analysis software Abaqus™ is used in this study. The finite element mesh of the carbide tip is shown in Fig. 5, which was modeled by 58,000 four-node hexahedral elements. 8*6 nodes are located on the projected contact length between the tool and the workpiece, 3 * 6 nodes are located on the chamfered width of the main cutting edge, and 1*6 nodes are placed on flank wear.

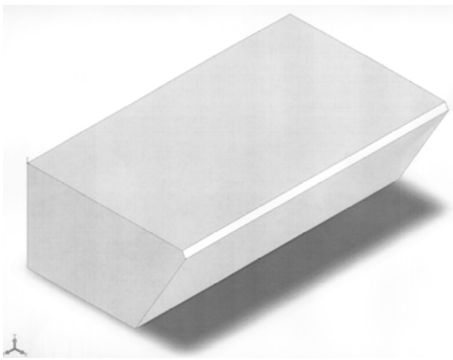

Figure 5. Solid model of the chamfered edge tool.

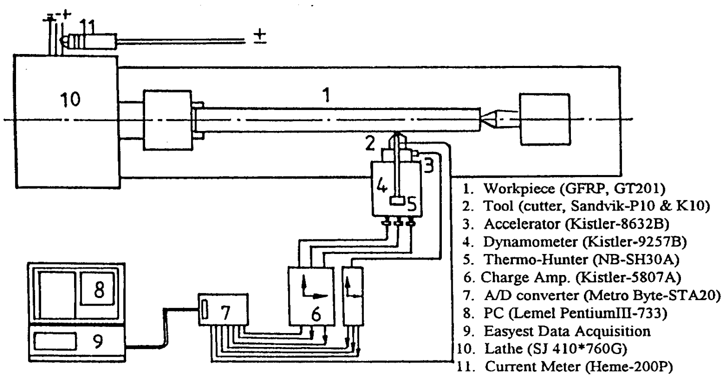


Figure 6. Experimental set-up.

### 2.5. Modified Carbide Tip Temperature Model

Magnitude of the tip's load is shown in the following Eqs. (32) and (33)

$K=U_f/A'$ (32) $A'=L_p(d+W_e+V_b)$ (33), $\rho c\frac{\partial T}{\partial t}=k\frac{\partial^2 T}{\partial x^2}+k\frac{\partial^2 T}{\partial y^2}+k\frac{\partial^2 T}{\partial z^2}$ (34)

where $\rho$ is the density, $c$ is the thermal conductivity, and $k$ is the heat capacity.

$q_{tool}=Kq_f$ Li and Shih (2005) (35), $Obj(K)=\sum_{i=1}^{ni}\sum_{j=1}^{nj}(T_j^{ti}|_{\exp}-T_j^{ti}|_{est})^2$ (2005) (36)

In this study, $K$ is assumed to be a constant for all cutting edges. The inverse heat transfer method is used to find the value of $K$ under certain turning speeds.

### 2.6. Inverse Heat Transfer Solution and Validation

The flowchart for inverse heat transfer solution of $K$ was obtained by the Abaqus™ solver and is summarized in Fig. 5. The inverse heat transfer method is applied to solve $K$ by minimizing an energy function on the tip surface determined by Eqs. (35)- (36) and finite element modeled temperature at specific infrared locations, as shown in Fig. 5 on the tip face. The discrepancy between the experimentally measured temperature by infrared pyrometer, j by time $t_i$, $T_j^{ti}\big|_{\exp}$ and finite element estimated temperature at the same infrared location and time, $T_j^{ti}\big|_{est}$ determines the value of the objective function.

## 3. EXPERIMENTAL METHODS AND PROCEDURES

Experimental set up is shown in Fig 6. The work material used was $0^\circ$; unidirectional filament wound fiber of CFRP with Vinylester resin composite materials in the form of bars having a diameter of 40 mm and 500 mm length by Liu (2002). Table 2 shows some of the physical and mechanical properties of CFRP prior to carrying out the cutting experiments. The cutting tools used in the experiments are Sandvik H1P (*K type*) by Brookes (1992). Tool composition: WC 85.5%, TiC 7.5%, Ta (Nb)C 1% and Co 6 %(30), $HV$ =1850, density=12.9 $g/cm^3$, thermal conductivity = 60 $W/m-^\circ K$ and heat capacity= 235 $J/Kg-^\circ K$.

## 4. RESULTS AND DISCUSSION

**4.1** From Fig. 7, it proved that the cutting edge temperature of the chamfered main edge tool was lower than unchamfered main cutting edge tool.

**4.2** According to Fig. 7, the tip temperatures of chamfered main cutting edge sharp worn tools were not high and the inverse (calculated) data correlates closely with the experimental values.

**4.3** From Fig.7, the cutting temperatures of chamfered main cutting edge sharp worn tool is the lowest, when $C_S = 20^\circ$, $\alpha_{S1}(\alpha_{S2}) = -10^\circ(10^\circ)$ and the temperature is not exceed $350℃$.

**4.4** From Fig.7, it proved that the distribution of chamfered main cutting edge sharp worn tool's temperature was close the Fig. 8.

## 5. CONCLUSIONS

The test investigated the cutting forces and cutting temperature during the turning of CFRP. Chamfered main cutting edge sharp worn tools with $C_S$ equals to 20 $\alpha_{S1}(\alpha_{S2}) = -10^{\circ}(10^{\circ})$ and nose radius $R$=0.3 mm, produce the lower cutting forces and lower cutting temperature. Good correlations between predicted values and experimental results of forces and temperatures during machining with chamfered main cutting edge sharp worn tools in cutting CFRP.

## APPENDIX

Coefficients of the tool have a sharp corner ($R = 0$) with tool wear

$$a_3 = \{[\frac{f\cos C_s}{\cos\alpha_{S2}} - W_e\cos\alpha_{S1} - \overline{CN}\cos(C_e - C_s)]^2[\tan\eta_c - \tan(C_e - C_s)]^2 + (f\cos C_s/\cos\alpha_e - W_e\cos\alpha_{s1} - \overline{CN}\cos(C_e - C_s))/\cos\eta_c]^2(\cos^2\alpha_e$$

$$\frac{(\frac{f\cos C_s}{\cos\alpha_e} - W_e\cos\alpha_{S1} - \overline{CN}\cos(C_e - C_s))}{\cos\eta_c}]^2(\cos^2\alpha_e(\tan\alpha_e + \cot\phi_e)^2 - 2[(f\cos C_s/\cos\alpha_e - W_e\cos\alpha_{s1} - \overline{CN}\cos(C_e - C_s))/\cos\eta_c]$$

$$\cos\alpha_e(\tan\alpha_e + \cot\varphi_e)\cos(0.5\pi - \alpha_b)\}^{1/2} \quad (1)$$

$$b_3 = [\frac{\frac{f\cos C_s}{\cos\alpha_{S2}} - W_e\cos\alpha_{S1} - \overline{CN}\cos(C_e - C_s)}{\cos\eta_c}]\frac{\cos\alpha_e}{\sin\phi_e} \; (2), \quad c_3 = [\frac{f\cos C_s/\cos\alpha_{s2} - W_e\cos\alpha_{s1})}{\cos(C_e - C_s)} - \overline{CN} \quad (3)$$

$$a_4 = d/\cos C_s - [f\cos C_s/\cos\alpha_{s2} - W_e\cos\alpha_{s1} - \overline{CN}\cos(C_e - C_s)]^2\,[\tan\eta_c - \tan(\eta_c - \tan(C_e - C_s)) - \overline{NM}\sin$$

$$(\pi - \angle CMN - \theta_B - \eta_c - C_e - C_s)/\sin(\theta_B - \eta_c + C_e - C_s) \; (4), \; b_4 = d/(\cos C_s - \cos C_e) - \overline{CM} \; (5); \quad h_4 = (c_4^{\,2} - d_4^{\,2})^{1/2} \; (6)$$

$$c_4 = [\frac{f\cos C_s - W_e\cos\alpha_{s1} - \overline{CN}\cos(C_e - C_s)}{\cos\eta_c} + [\frac{\overline{NM}\sin(\pi - \theta_B - \angle CNM)}{\sin(\theta_B - \eta_c + C_s - C_e)}]\frac{\cos\alpha_e}{\sin\varphi_e} \quad (7)$$

$$a_5 = \overline{NM} \quad b_5 = b_3 \quad c_5 = a_3, \quad e_5 = [\frac{f\cos C_s}{\cos\alpha_{S1}} - W_e\cos\alpha_{S1} - \overline{CN}\cos(C_e - C_s)][\tan\eta_c - \tan(C_e - C_s)] \quad (8)$$

$$d_5 = [\frac{(\frac{f\cos C_s}{\cos\alpha_e} - W_e\cos\alpha_{S1} - \overline{CN}\cos(C_e - C_s)}{\cos\eta_c}]\cos\alpha_e(\tan\alpha_e + \cot\phi_e) \quad (9)$$

$$g_5 = [\frac{f\cos C_s/\cos\alpha_{s2} - W_e\cos\alpha_{s1} - \overline{CN}\cos(C_e - C_s)}{\cos\eta_c} + [\frac{\overline{NM}\sin(\pi - \theta_B - \angle CNM)}{\sin(\theta_B - \eta_c + C_s - C_e)}]\frac{\cos\alpha_e}{\sin\varphi_e} \quad (10)$$

$$h_5 = (m_5^2 + n_5^2 - 2m_5 n_5 \sin\alpha_b)^{1/2} \quad (11)$$

$$m_5 = \frac{\overline{NM}\sin(\pi - \theta_B - \angle CNM + \eta_c - C_e + C_s)}{\sin(\theta_B - \eta_c + C_e - C_s)} \quad (12), \quad n_5 = g_5 \sin\phi_e(\tan\alpha_e + \cot\phi_e) - d_5 \quad (13)$$

$$l_5 = [\frac{f\cos C_s}{\cos\alpha_{S1}} - W_e\cos\alpha_{S1} - \overline{CN}\cos(C_e - C_s)](\tan\eta_c - \tan(C_e - C_s)) - \overline{CM} + \frac{\overline{NM}\sin(\pi - \theta_B - \angle CNM + \eta_c - C_e + C_s)}{\sin(\theta_B - \eta_c + C_e - C_s)} \quad (14)$$

$$s_5 = (l_5^2 + r_5^2 - 2l_5 r_5 \sin\alpha_b)^{1/2} \quad (15), \quad r_5 = g_5 \sin\varphi_e(\tan\alpha_e + \cot\varphi_e)/\cos\alpha_e \quad (16)$$

## REFERENCES


Bhatnagar, N., Ramakrishnan, N., Naik, N.K., Komanduri, R., 1995, “On the machining of fiber reinforced plastic(FRP) composite laminates,” *International Journal of Machine Tools and Manufacture*, pp. 701–716.

Brookes, K.J.A., World directory and handbook of hard metals, 5th ed., *International carbide data hand book*”, United Kingdom, 1992, pp. 172−175.

Chang, C.S., 2008, "Prediction of cutting temperatures in turning of glass-fiber-reinforced plastics with chamfered main cutting edge tools," *Journal of Mechanics*, Vol. 24, pp. 241–252.

Li, R., Shih, A.J., *Inverse heat transfer solution in tool temperature titanium drilling, mechanical engineering*, University of Michigan Ann Arbor, 2005.

Liu, C.C., *FRP composites*, Golden Talent Industries Co. Ltd., Hsin-Chu, Taiwan, R.O.C., 2002

Rosen, B.W., Dow, N.F., Overview of composite materials, Analysis and design, in: *Engineered Materials Handbook*, American Society for Metals, 1987, pp. 175−180.

Reklaitis, G.V., Ravindran, A., Ragsdell, K.M., *Region-elimin method, engineering optima. methods and application*, Willy, Inc., New York, pp. 37−38, 1984 .

Singamneni, S.B., 2005, “A mixed solution for three-dimensional temperature distribution in turning inserts using finite and boundary element techniques,” *Journal of Materials Processing Technology*, Vol. 166, pp. 98−106.

# ACKNOWLEDGEMENT

This work was supported by National Science Council, Taiwan, R.O.C. under grant number NSC 2008-2622-E-197-001-C

Table 1. Tool geometry specifications (chamfered main cutting edge)

| side cutting edge angle $C_S$ | tool no | side rake angles $\alpha_{S1}, \alpha_{S2} (\alpha_{r1}, \alpha_{r2})$ | Nose roundness ( R) | carbide tool |
|---|---|---|---|---|
| 20 ° | 1 | 10°, -10° ( 10 ° , -10 ° ) | 0.0, 0.1 (sharp and worn) | K10 |
| 20 ° | 2 | 30°, -30 ° (30 ° , -30 ° ) | 0.0, 0.1 (sharp and worn) | K10 |
| 30 ° | 3 | 10°, -10 ° (10 ° , -10 ° ) | 0.0, 0.1 (sharp and worn) | K10 |
| 30 ° | 4 | 30°, -30 ° (30 ° , -30 ° ) | 0.0, 0.1 (sharp and worn) | K10 |
| 40 ° | 5 | 10°, -10 ° (10 ° , -10 ° ) | 0.0, 0.1 (sharp and worn) | K10 |
| 40 ° | 6 | 30°, -30 ° (30° , -30 ° ) | 0.0, 0.1 (sharp and worn) | K10 |
| notation: tool holder & tips | | 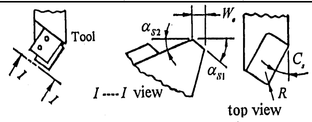  | | |

Table 2. Properties of the work materials (roving continuous strand, hardness, HS: 55~60)

| density g/cm$^3$ | thermal conductivity kCal/hr°C | fiber contain | thermal expansion ($10^{-6}$ /°C) | tensile strength (kg/cm$^2$) | compressive strength (kg/cm$^2$) | shear strength (kg/cm$^2$) | modulus tensile (kg/cm$^2$) |
|---|---|---|---|---|---|---|---|
| 1.7~1.9 | 0,21~0.28 | 75% | 2~9 | 3.5~4 | 3.5~3.9 | 1.5~2 | 235~400 |

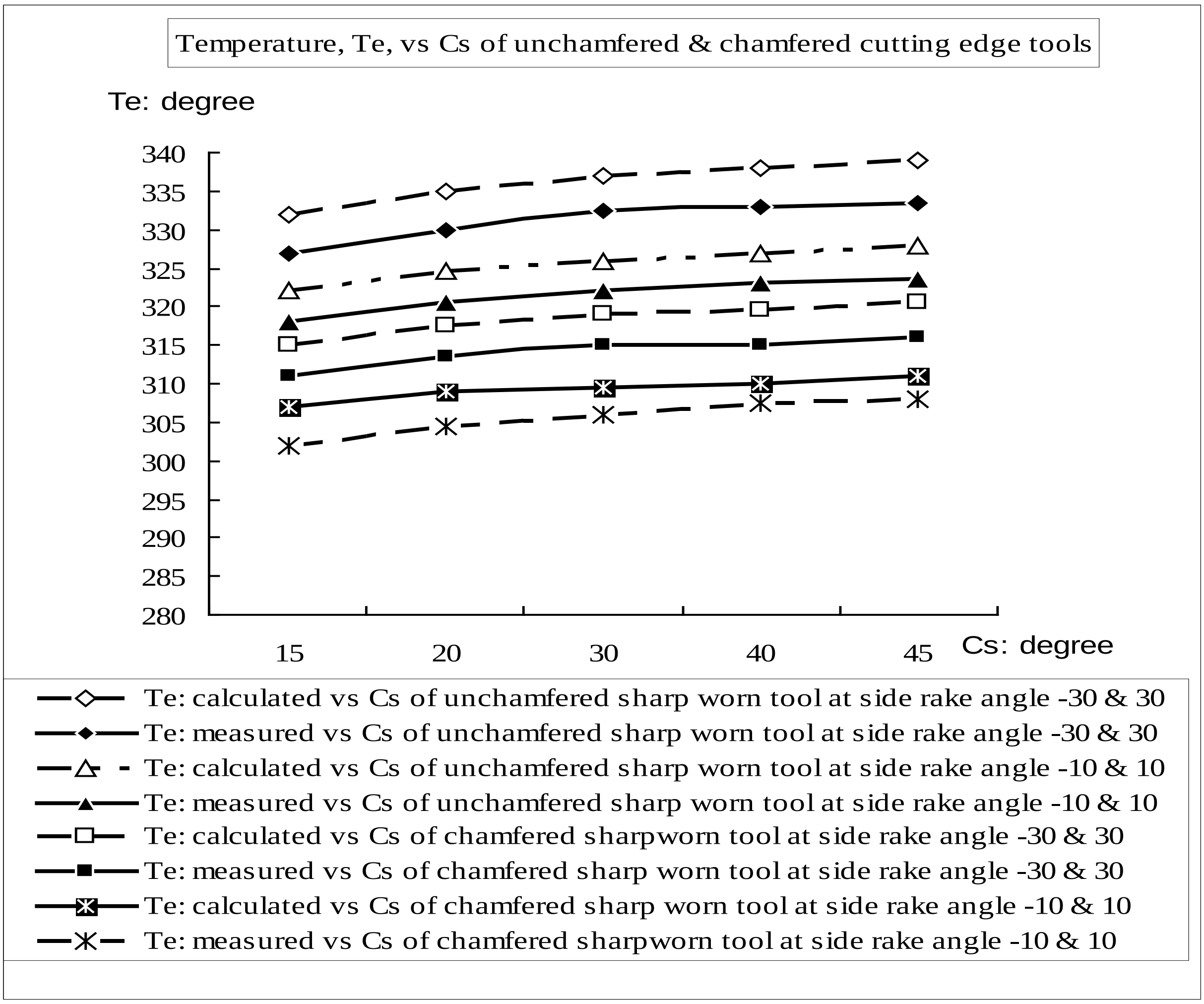


Figure 7. Shows the cutting temperatures vs $C_S$ for different values $\alpha_{S1}$ and $\alpha_{S2}$ with chamfered and unchamfered sharp tool at d=3.0 mm, f=.33 mm/rev, V=252m/min respectively.

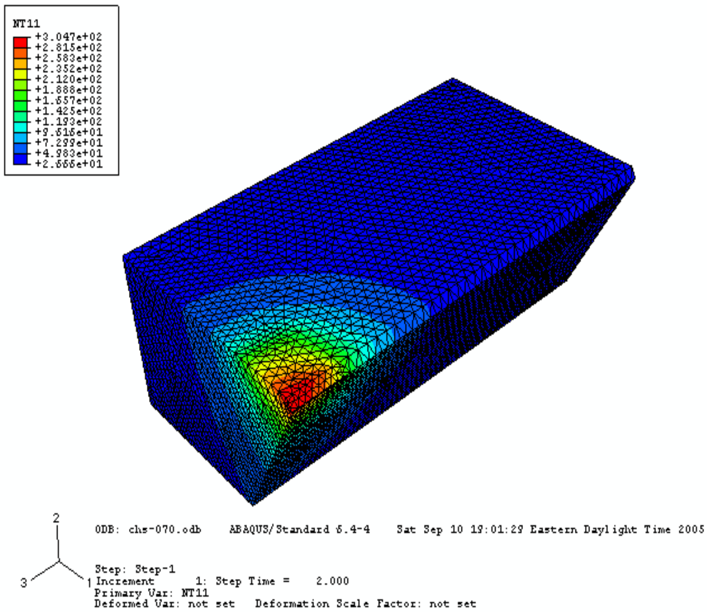


(a)

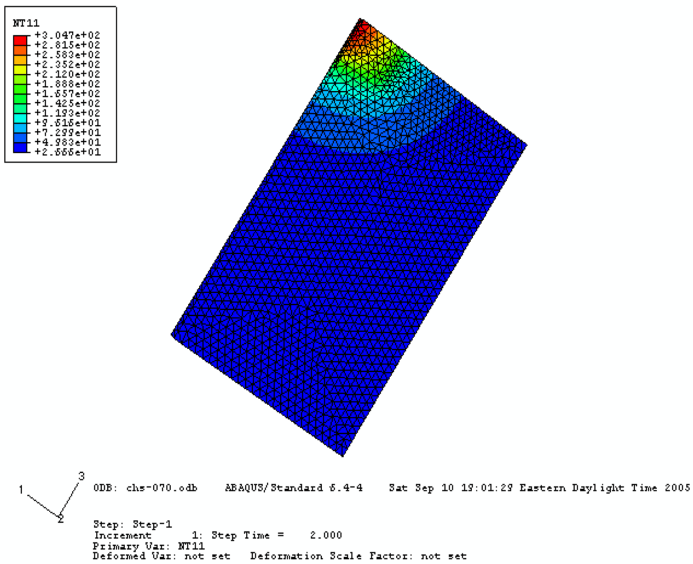


(b)

Figure 8. Temperature distribution with chamfered cutting edge inserts (a) heat flux (b) near the tool nose at $C_S$ = 30°, $\alpha_{S1}(\alpha_{S2}) = -10^{\circ}(10^{\circ})$, d=3.0 mm, f=0.33 mm/rev, and V=252 m/min (GFRP)